blocks of length Δl; the total number of such blocks corresponded to the number of flattened passbands desired. These masks could also be moved relative to the reference mask in order to properly position the Δl regions for eliminating the desired FP resonances.

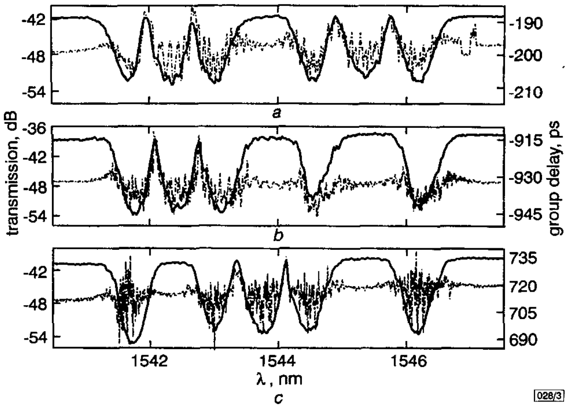

Fig. 3 *Experimentally measured transmission spectra of CMGs designed to have single or multiple flattened passbands*

- - - - group delay
——— spectra
a Single region Δl = 0.5cm placed in middle of grating yielding single flattened passband at centre of transmission response
b Two regions $\Delta D l_1$ = 0.5cm and Δl_2 = 0.6cm placed, respectively, in middle of grating and 0.4cm from the end of the grating on long wavelength side yielding two flattened passbands side-by-side
c Two regions $\Delta D l_1 = \Delta l_2$ = 0.6cm placed 0.4cm from the two ends of the grating yielding two separate flattened passbands at the two edges of the transmission response

We calculated the transmission spectrum of a 3.5cm long CMG with a grating period chirp of 0.5mn/cm (corresponding to the mask chirp), $\Delta\lambda$ = 0.16nm, and a peak index modulation of 5×10^{-4}; for this design, there are six passbands. To eliminate two consecutive FP resonances, Δl should be 0.5–0.6cm long. Thus, depending on the number of Δl regions, we can obtain one to three flattened passbands from the original CMG. We can also set the wavelength positions of the passbands by changing the positions of the Δl regions. Choosing to eliminate more than two consecutive FP resonances would simply result in a flattened passband with a larger BW. Fig. 2 illustrates effects of placing regions of no index modulation on 3.5cm long CMG with grating period chirp of 0.5nm/cm, $\Delta\lambda$ = 0.16nm, and peak index modulation of 5×10^{-4}. The FWHM BW of the flattened passbands ($\simeq$ 0.73nm) corresponds to the width between consecutive FP resonances of the original CMG. We can also see the FP resonances that have not been eliminated.

The gratings were written using 248 nm radiation from a KrF excimer laser in Corning SMF-28 fibre which had been hydrogen-loaded ~ 125atm at room temperature for more than 10 days. Once the appropriate amplitude masks which yield the desired transmission response were positioned behind the phase mask, we then scanned the UV beam across the amplitude/phase mask combination, placed the fibre under strain, and performed a second scan. Both scans were made at the same speed (0.15mm/s), pulse repetition rate (50Hz), and pulse energies (50–60mJ/pulse).

Fig. 3 shows the experimentally measured transmission spectra (obtained using a tunable laser diode with 10 pm resolution) of CMGs fabricated with one or two flattened passbands corresponding to those in Fig. 2. The agreement between the calculated and measured results is excellent, indicating the feasibility for fabricating such structures. The passbands have a ripple of < 0.5dB and exhibit > 12dB isolation. Another important property of these filters is the near-constant in-band group delay which is also shown in Fig. 3. The amount of channel isolation depends on the strength of the gratings written and we expect higher values for stronger gratings. Note that, unlike the simulations, the multiple passbands do not have the same BW. In fact, the FP resonances have unequal spacings which increase with wavelength. Experiments show that this effect is due to imperfections in the phase mask. Nonetheless, we were still able to obtain filters with the desired flattened passbands.

In summary, we have fabricated transmission filters with single or multiple flattened passbands based on CMGs by using amplitude masks in conjunction with a dual-exposure technique. The experimental results are in excellent agreement with simulations thus showing the feasibility of this technique for fabricating various transmission filters which can be tailored to suit the needs of WDM systems.

Acknowledgment: We thank J. Kalbfleisch for micromachining the amplitude masks and M.M. Ohn (Electrophotonics Corporation) for group delay measurements. This research was supported by grants from the Natural Sciences and Engineering Research Council of Canada (NSERC) and Photonics Research Ontario. L.R. Chen thanks NSERC and the Walter C. Sumner Foundation for financial assistance.

22 January 1999
Electronics Letters Online No: 19990406
DOI: 10.1049/el:19990406

L.R. Chen, H.S. Loka, D.J.F. Cooper and P.W.E. Smith (*Department of Electrical and Computer Engineering, University of Toronto and Photonics Research Ontario, 10 King's College Road, Toronto, Ontario M5S 3G4, Canada*)

E-mail: chenl@ecf.utoronto.ca

H.S. Loka: Currently with the Engineering Physics Department, Cairo University, Cairo, Egypt

R. Tam and X. Gu (*Photonics Research Ontario, 60 St. George Street, Suite 331, Toronto, Ontario M5S 1A7, Canada*)

References

1 TOWN, G.E., SUGDEN, K., WILLIAMS, J.A.R., BENNION, I., and POOLE, S.B.: 'Wideband Fabry-Pérot-like filters in optical fibre', *IEEE Photonics Technol. Lett.*, 1995, **7**, pp. 78–80

2 EVERALL, L.A., SUGDEN, K., WILLIAMS, J.A.R., BENNION, I., LIU, X., AITCHISON, J.S., and DE LA RUE, R.M.: 'Fabrication of multipassband moire' resonators in fibres by the dual-phase-mask exposure method', *Opt. Lett.*, 1997, **17**, pp. 1473–1475

3 CHEN, L.R., COOPER, D.J.F., and SMITH, P.W.E.: 'Transmission filters with multiple flattened passbands based on chirped Moiré gratings', *IEEE Photonics Technol. Lett.*, 1998, **10**, pp. 1283–1285

4 CHEN, L.R., and SMITH, P.W.E.: 'Fibre Bragg grating transmission filters with near-ideal filter response', *Electron. Lett.*, 1998, **34**, pp. 2048–2050

Gratings photowritten in ion-exchanged glass channel waveguides

D.F. Geraghty, D. Provenzano, W.K. Marshall, S. Honkanen, A. Yariv and N. Peyghambarian

Gratings are photowritten in ion-exchanged glass channel waveguides. The transmission of these waveguides shows a rejection dip of almost 20dB. The polarisation dependence of these waveguide gratings is measured and discussed.

Both integrated optics and grating-based waveguide devices have demonstrated vast capabilities in the areas of sensors and telecommunications. These two technologies have been successfully combined as Bragg gratings which have been fabricated in both germanium-doped silica [1] and sol-gel [2] glass channel waveguides.

Ion-exchanged glass waveguides have proven their viability and are currently used in commercially available passive devices. Photowritten gratings have been demonstrated in ion-exchanged glass slab waveguides [3]; however, in that work gamma-ray irradiation was required to create an absorption defect for the photosensitivity and the glass used was from an experimental melt. Additionally, gratings have been relief etched into ion-exchanged glass channel waveguides [4]. However, etched gratings are limited to surface waveguides; they intrinsically introduce additional loss, and they suffer from a severe polarisation dependence of their reflectivity [5].

In this Letter, we demonstrate gratings photowritten in commercial ion-exchanged glass channel waveguides. Surface waveguides are used here, but the technique is also applicable for buried waveguides. The transmission of the waveguides is analysed, the polarisation dependence characterised, and avenues for future improvements are discussed.

BGG31 glass is used for the channel waveguides [6]. The composition of BGG31 is optimised for silver ion-exchange waveguide fabrication, not for photosensitivity. BGG31 is currently used for the fabrication of commercially available ion-exchanged passive waveguide devices. This demonstration of its photosensitivity opens a new realm of possibilities for this glass that has already proven itself an excellent glass waveguide material.

Surface waveguides were formed in the BGG31 glass by silver ion-exchange. The waveguides were formed by patterning a 200nm thick Ti mask with straight waveguides of varying widths. The mask was oxidised for 1h in an $NaNO_3$ salt melt at 380°C. The sample was then placed into an $AgNO_3$ salt melt at 300°C for 15min. Finally, the mask was removed and the end facets were polished.

The grating was photowritten using a 248nm excimer laser. An area of 2cm × 2mm was exposed through a phase mask with a periodicity of 1049.28nm. With the laser operating at a pulse rate of 50Hz with 168mJ/pulse, the 10min exposure gave a total exposure energy of 5040J.

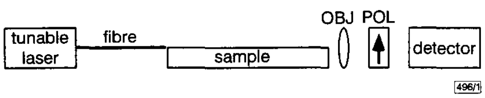

Fig. 1 *Setup for transmission characterisation*

Fig. 1 shows the setup used for testing the grating. The fibre output of a tunable laser was butt-coupled to the input of the channel waveguide. The waveguide output was collimated with a ×20 objective and then passed through a polariser, to enable detection of the TE and TM components separately. The power was then monitored with a detector as the input wavelength was tuned.

The TE transmission of an 8μm wide waveguide with the grating is shown in Fig. 2. The peak rejection ratio is 19.19dB. Although this is quite good, it should be possible to further improve the rejection by better alignment of the grating with the waveguide, a longer exposure, or a longer grating. The sidelobe of the grating is most likely due to some asymmetry in the writing process. There are some additional dips (not shown in the Figure) in the transmission at ~ 2nm away. We believe that this is due to coupling to a higher order mode of the waveguide resulting from imperfect alignment of the grating to the waveguide. A more precise alignment of the grating perpendicular to the waveguide should eliminate these additional dips in the transmission.

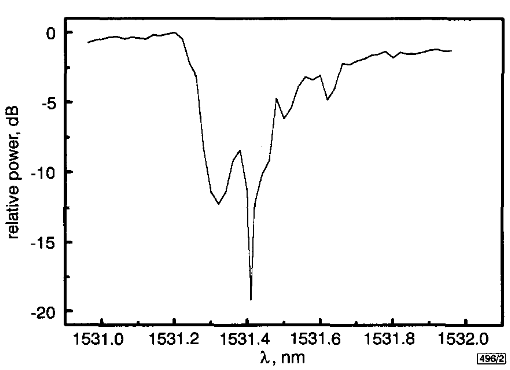

Fig. 2 *TE transmission of 8μm wide waveguide with grating*
Peak rejection is 19.19dB down

These surface waveguides are birefringent, resulting in different effective indices for the TE and TM modes at the same wavelength. Consequently, the transmission dip for the different modes will occur at different wavelengths. The measured polarisation dependence of the transmission of the waveguides with the grating is shown in Fig. 3. Here the characterisation is performed as shown in Fig. 1 except that an optical spectrum analyser with 0.1nm resolution bandwidth is used in place of the detector. This results in the measurement equivalent of a broadband source and a detection resolution larger than the feature size of the grating. The finite resolution bandwidth reduces the measured peak rejection and also changes the shape measured.

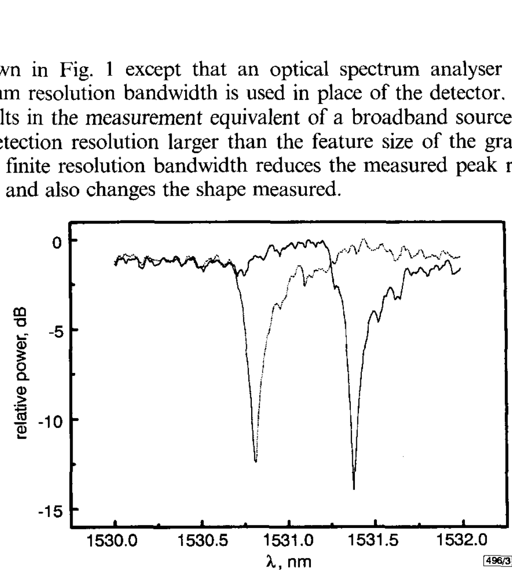

Fig. 3 *Comparison of TE and TM transmission*
——— TE
.... TM

The TE-TM shift in wavelength of the peak rejection is measured to be 0.56nm. This agrees reasonably well with the 0.69nm shift which was predicted by simple modelling of the ion-exchanged waveguides. This polarisation dependence should be easily removable by fabricating non-birefringent double ion-exchanged waveguides [7]. It should also be noted that there is no strong polarisation dependence to the magnitude of the transmission dip, as seen previously with etched gratings [5].

In conclusion, gratings with strong transmission dips of almost 20dB have been photowritten in ion-exchanged glass channel waveguides. This technique should allow for low-loss, polarisation insensitive gratings to be written in either surface or buried ion-exchanged glass channel waveguides. Such devices would have numerous applications in many areas, including sensors and telecommunications.

Acknowledgments: We wish to thank Integrierte Optik GmbH, Waghäusel-Kirrlach, Germany, for providing the glass substrates. We also thank S.B. Mendes for help in the waveguide fabrication process.

17 February 1999
Electronics Letters Online No: 19990391
DOI: 10.1049/el:19990391

D.F. Geraghty (*NP Photonic Technologies, UA Science and Technology Park, 9030 S. Rita Rd., Suite 120, Tucson, AZ 85747, USA*)

D. Provenzano, W.K. Marshall and A. Yariv (*California Institute of Technology, Applied Physics Dept., Mail Code 128-95, Pasadena, CA 91125, USA*)

S. Honkanen and N. Peyghambarian (*University of Arizona, Optical Sciences Center, 1630 E. University Blvd., Tucson, AZ 85721, USA*)

References

1 ALBERT, J., BILODEAU, F., JOHNSON, D.C., HILL, K.O., MIHAILOV, S.J., STRYCKMAN, D., KITAGAWA, T., and HIBINO, Y.: 'Polarisation-independent strong Bragg gratings in planar lightwave circuits', *Electron. Lett.*, 1998, **34**, (5), pp. 485–486

2 TOUAM, T., DU, X.M., FARDAD, M.A., ANDREWS, M.P., and NAJAFI, S.I.: 'Sol-gel glass waveguides with Bragg grating', *Opt. Eng.*, 1998, **37**, (4), pp. 1136–1142

3 ROMAN, J.E., and WINICK, K.A.: 'Photowritten gratings in ion-exchanged glass waveguides', *Opt. Lett.*, 1993, **18**, (9), pp. 808–810

4 LI, M.J., HONKANEN, S., WANG, W.J., LEONELLI, R., ALBERT, J., and NAJAFI, S.I.: 'Potassium and silver ion-exchanged dual-core glass waveguides with gratings', *Appl. Phys. Lett.*, 1991, **58**, (23), pp. 2607–2609

5 LI, M.J., and NAJAFI, S.I.: 'Polarization dependence of grating-assisted waveguide Bragg reflectors', *Appl. Opt.*, 1993, **32**, (24), pp. 4517–4521

6 FABRICIUS, N., OESTE, H., GUTTMANN, H.-J., QUAST, H., and ROSS, L.: 'BGG 31: A new glass for multimode waveguide fabrication'. EFOC/LAN 88, Amsterdam, 1988

7 ÄYRÄS, P., NUNZI CONTI, G., HONKANEN, S., and PEYGHAMBARIAN, N.: 'Birefringence control for ion-exchanged channel glass waveguides', *Appl. Opt.*, 1998, **37**, (36), pp. 8400–8405

Indicator of amplified spontaneous emission in erbium doped fibre amplifiers

Fu-Sjun Lai, Jau-Ji Jou and Cheng-Kuang Liu

The influence of amplified spontaneous emission (ASE) on the performance of erbium doped fibre amplifiers (EDFAs) has been studied through the use of an ASE indicator, the nearly-no-ASE factor (NNAF). A simple and useful formula is also presented for the analysis of errors resulting from neglecting the ASE.

Introduction: In the applications of fibres to communications and sensor systems, the EDFA plays an essential role in boosting power or preamplifying signals [1 – 5]. The prediction of EDFA performance is important in system design or analysis, but it becomes complicated if ASE [6] is taken into account. A simple method for determining, in a quantitative way, the degree of the influence of ASE can be helpful. We have studied the effect of AHE on EDFA gains and found that the ASE can be neglected when the NNAF is large enough. It is proposed as an ASE indicator. Moreover, a formula for computing the errors in output power due to neglecting ASE in the calculations is also presented.

Theory: Assume that the excited-state absorption can be neglected and the temporal variations of the atomic populations are slow in comparison with the transit time of the pump and signal through the unidirectional-pump two-level EDFA system. The rate equation for the population N_2 in the metastable level and the evolution of pump power P_p, signal power P_s, forward and backward z-propagating ASE powers $P_l^{\pm}$ at optical frequency ν_l and in frequency interval $\Delta\nu_l$, can be written as

$$\frac{\partial N_2}{\partial t} = -\left(\sum_{j=s,p,l} \frac{\sigma_{jae}\Gamma_j}{A} P_j + \frac{1}{\tau}\right) N_2 + \sum_{j=s,p,l} \frac{\sigma_{ja}\Gamma_j}{A} P_j N_t \tag{1}$$

$$\frac{\partial P_k}{\partial z} = \Gamma_k(\sigma_{kae}N_2 - \sigma_{ka}N_t)P_k \tag{2}$$

$$\frac{\partial P_l^{\pm}}{\partial z} = \pm\Gamma_l\left[(\sigma_{lae}N_2 - \sigma_{la}N_t)p_l^{\pm} + 2h\nu_l\Delta\nu_l\sigma_{le}N_2\right] \tag{3}$$

where the power is in units of photon/s, $k = s$ and p for signal and pump powers, $\sigma_{jae} = \sigma_{ja} + \sigma_{je}$ for $j = k$ and l, $P_l = P_l^+ + P_l^-$, N_t is the erbium density in the fibre core of effective area A, τ is the fluorescence lifetime of the metastable level, σ_{ka} and σ_{la} are the absorption cross-sections at wavelengths λ_k and λ_l, respectively, the corresponding emission cross-sections are σ_{ke} and σ_{le}, Γ_s, Γ_p and Γ_l are the overlap factors of signal, pump, and ASE powers, respectively. For an EDFA with erbium-doped fibre of length L, eqns. 1 – 3 lead to the following expression for steady-state input and output powers $P_{k0}^{in,out}$:

$$\ln\frac{P_{k0}^{out}}{P_{k0}^{in}} = \frac{1}{P_k^{IS}}\left[\sum_{j=s,p}(P_{j0}^{in} - P_{j0}^{out}) + \sum_l (P_l^+(l) + P_l^-(0))\right] - \alpha_k L$$

with $\alpha_k = \Gamma_k\sigma_{ka}N_t$ and $P_k^{IS} = A/(\Gamma_k\sigma_{kae}\tau)$. Considering the ratio of power available for the signal gain to ASE power we define the NNAF as

$$NNAF = \left[1 + \frac{P_s^{IS}\ln G}{P_s^{IS}\alpha_s L - \sum_{j=s,p}(P_{j0}^{in} - P_{j0}^{out})}\right]^{-1} \tag{4}$$

where $G = P_{s0}^{out}/P_{s0}^{in}$. It is in closed form and can be calculated simply. Also, its dependence on input signal power is almost linear, as will be shown below. It is thus proposed as an ASE indicator.

A large NNAF indicates little ASE effect on the signal gain. The percentage error of output power due to neglecting ASE in the calculation can be computed as $R_s = (P_{sn}^{out} - P_{s0}^{out})/P_{sn}^{out}$, where P_{sn}^{out} and P_{s0}^{out} denote the signal powers calculated without and with the inclusion of ASE. Since

$$NNAF = \frac{\left[1 - \frac{(1-R_s)\ln G}{(1-R_s)\ln(1-R_s)+R_sP}\right]}{\left[1 + \frac{R_s\ln G}{(1-R_s)\ln(1-R_s)+R_sP}\right]}$$

where $P = \alpha_s L - \Sigma_{j=s,p}(P_{j0}^{in}/P_s^{IS})$, we have

$$R_s \simeq 1 - P - \ln G - \sqrt{[P + \ln G - 1]^2 - \frac{2\ln G}{NNAF - 1}} \tag{5}$$

When R_s is small, simple formulas [3, 6] derived under the ASE-free assumption can be applied and the analysis of EDFA performance becomes simple and accurate enough.

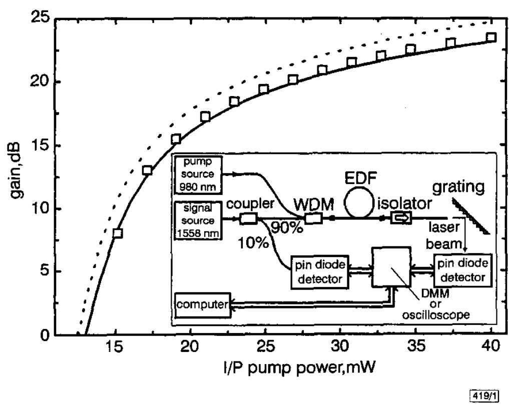

Fig. 1 *Measured and calculated gains against pump power for EDFA with 12m erhium-doped fibre and 50μW input signal*

Inset: schematic diagrams of experimental setup
- - - - without ASE
——— with ASE
□ experiment

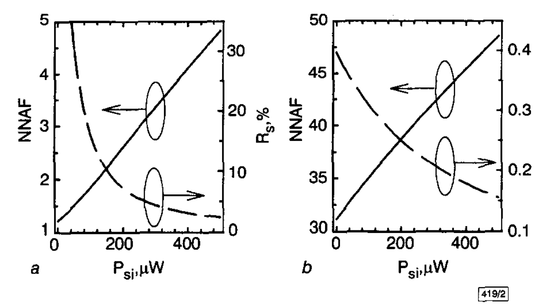

Fig. 2 *NNAF and error R_s against signal power for 12m and 1m EDFAs with 40mW pump power*

a 12m
b 1m

Results and discussion: To verify our method, measurements for a 980 nm-pump EDFA were made using the experimental setup of [7], as schematically shown as an inset to Fig. 1. Calculated and measured gains are shown in Fig. 1 against pump power. The erbium-doped fibre length is 12m. The input signal is 50μW. Other parameters used are: $N_T = 7.7 \times 10^{24}$m^{-3}, τ = 10ms, $A = 2.5 \times 10^{-11}$m^2, $\sigma_{sa} = 2.4 \times 10^{-25}$m^2, σ_{se} 3.8×10^{-25}m^2, $\sigma_{pa} = 2.0 \times 10^{-25}$m^2, and NA = 0.18. It shows that the agreement between the calculation and measured gains is good when the ASE is included in our calculation. One way to determine the degree of ASE influence on signal gain is to apply the finite difference method to solve eqns. 1 – 3. For instance, an error R_s(FD) = 30.1% in the output signal